RSC Advances

PAPER

View Article Online
View Journal | View Issue

Cite this: *RSC Adv.*, 2015, **5**, 90428

Poly(vinylidene fluoride-*co*-chlorotrifluoroethylene) (PVDF-CTFE) lithium-ion battery separator membranes prepared by phase inversion†

R. E. Sousa,[a] Manab Kundu,[b] A. Gören,[ac] M. M. Silva,[c] Lifeng Liu,[b] C. M. Costa*[ac] and S. Lanceros-Mendez[a]

Received 19th September 2015
Accepted 15th October 2015

DOI: 10.1039/c5ra19335d

www.rsc.org/advances

Separator membranes based on poly(vinylidene fluoride-*co*-chlorotrifluoroethylene) (PVDF-CTFE) were prepared by a solvent casting technique based on its phase diagram in *N*,*N*-dimethylformamide (DMF) solvent. The microstructure of the PVDF-CTFE separator membranes depends on the initial position (temperature and concentration) of the solution in the phase diagram of the PVDF-CTFE/DMF system. A porous microstructure is achieved for PVDF-CTFE membranes with solvent evaporation temperatures up to 50 °C for a polymer/solvent relative concentration of 20 wt%. The ionic conductivity of the separator depends on the degree of porosity and electrolyte uptake, the highest room temperature value being 1.5 mS cm^{-1} for the sample with 20 wt% of polymer concentration and solvent evaporation temperature at 25 °C saturated with 1 mol L^{-1} lithium bis(trifluoromethanesulfonyl) imide (LiTFSI) in propylene carbonate (PC). This PVDF-CTFE separator membrane in Li/C–$LiFePO_4$ half-cell shows good cyclability and rate capability, showing a discharge value after 50 cycles of 92 mA h g^{-1} at 2C, which is still 55% of the theoretical value. PVDF-CTFE separators are thus excellent candidates for high-power and safe lithium-ion battery applications.

Introduction

Rechargeable lithium-ion batteries with higher energy density and safety are necessary taking into account the rapid technological development in applications such as mobile phones, computers, e-labels, e-packaging, disposable medical testers, hybrid electric vehicles (PHEVs) and electric vehicles (EVs).[1,2]

Rechargeable lithium-ion batteries are one of the most efficient technologies for energy storage[3–5] due to their excellent characteristics: they are light, cheap, show high energy density (210 W h kg^{-1}), low self-discharge rate (2–8% per month), no memory effect, prolonged service-life and high number of charge/discharge cycles (>1000 cycles), high-operation voltage (2.5–4.2 V) and capability to store 2–3 times the energy per unit weight and volume when compared to Ni–Cd rechargeable batteries.[3,6–8]

The basic constituents present in a lithium-ion battery are the anode, cathode and the electrolyte separator. The electrolyte separator separates anode and cathode and serves as the medium for the transfer of charges, preventing internal short circuit and providing a pathway for ionic conduction in the liquid electrolyte.[9–12] The electrolyte separator can be constituted by a porous polymer matrix in which the membrane is soaked by the electrolyte solution, *i.e.*, a liquid electrolyte where lithium salts are dissolved in solvents, water or organic molecules. More recently, a new type of electrolyte based in organic ionic plastic crystals has been shown to improve the durability of electrochemical devices such as batteries.[13,14] Other possibility for the fabrication of the polymer electrolyte separators is the incorporation of the lithium salts directly in the polymer matrix.[15]

An ideal separator should have an low ionic resistance and dimensional stability at elevated temperatures.[8]

Different polymer matrices have been used as separators[12,16–18] such as poly(ethylene oxide) (PEO),[19] poly(acrylonitrile) (PAN),[20] poly(methyl methacrylate) (PMMA),[21] poly(vinyl chloride) (PVC),[22] poly(vinylidene fluoride) (PVDF)[23] and its copolymers, poly(vinylidene fluoride-hexafluoropropylene) (PVDF-HFP),[24] poly(vinylidenefluoride-*co*-trifluoroethylene), (PVDF-TrFE)[25] and poly(vinylidene fluoride-*co*-chlorotrifluoroethylene) (PVDF-CTFE)[26] and more two recent matrizes: ethylcellulose-coated polyolefin[27] and expanded polytetrafluoroethylene reinforced polyvinylidene-fluoride-hexafluoropropylene.[28]

PVDF and its copolymers have excellent properties for being used as a separator membrane in comparison with others polymer matrixes.[12] These properties include high polarity, high dielectric constant, low degree of crystallinity, morphology

[a]*Departamento/Centro de Física, Universidade do Minho, Campus de Gualtar, 4710-057 Braga, Portugal. E-mail: cmscosta@fisica.uminho.pt*

[b]*International Iberian Nanotechnology Laboratory (INL), Av. Mestre Jose Veiga, 4715-330 Braga, Portugal*

[c]*Departamento/Centro de Química, Universidade do Minho, Campus de Gualtar, 4710-057 Braga, Portugal*

† Electronic supplementary information (ESI) available. See DOI: 10.1039/c5ra19335d

control through binary and ternary polymer/solvent phase diagram, good wettability and electrochemical stability due to the presence of a strong electron-withdrawing group (C–F).

PVDF-CTFE is the less studied co-polymer of PVDF for use as battery separators,[12] despite its interesting characteristics.[29] PVDF-CTFE shows interesting characteristics (high electromechanical response, high flexibility, high elongation and cold impact resistance) in comparison of other co-polymers of PVDF.[29]

PVDF-CTFE has been prepared by electrospinning with[30] and without fillers[26] but the battery performance was only evaluated in Sn–C/PVDF-CTFE/$LiNi_{0.5}Mn_{1.5}O_4$ cells for the material without fillers. It is claimed that this polymer guarantees environmental sustainability, high energy content, and low safety hazard, and shows stable behavior with a capacity decay, for cycles run at rates lower than 1C, of just 0.06 mA h g^{-1} per cycle.[26]

Other works with PVDF-CTFE polymer for battery separator membranes involve nanofiber-coated polypropylene (PP) separator membranes.[31,32] It is shown that electrolyte uptake and separator–electrode adhesion are improved by the nanofiber coatings. The improvement in electrolyte uptake is not just related to the gelation capability of the PVDF-CTFE nanofibers, but also attributed to the porosity and capillary effect on nanofibrous structure.[31] Thus, in these works the electrochemical properties and battery performance of PVDF-CTFE polymer are not presented.

Taking into account the poor state-of-the-art for this interesting co-polymer, the main goal of this work is to prepare PVDF-CTFE membranes with different microstructures and to correlate them with battery performance. The different microstructures (*i.e.*, pore size and degree of porosity) are obtained by solvent casting of the binary polymer/solvent (*N*,*N*-dimethylformamide, DMF) systems varying systematically polymer concentration and solvent evaporation temperature.[29]

Morphology, thermal, mechanical and electrical properties were investigated for the different PVDF-CTFE membranes, together with battery performance in high-rate capability and cycle life in Li/C–$LiFePO_4$ half-cells.

Experimental

Materials

Poly(vinylidene fluoride-*co*-chlorotrifluoroethylene) PVDF-CTFE (Solef 31 508; $M_w = 270$–290 kg mol^{-1}; 18.66 wt% CTFE content) was supplied by Solvay. The solvents *N*,*N*-dimethylformamide (DMF, 99.5%), propylene carbonate (PC) and lithium bis(trifluoromethanesulfonyl) imide, LiTFSI were purchased from Merck and Sigma-Aldrich, respectively.

Separator membrane preparation

The different experimental steps involved in the PVDF-CTFE membrane preparation are shown in Fig. 1, indicating also relevant parameters such as processing time and temperature.

In the solution preparation step, PVDF-CTFE polymer concentrations in solution of 5 wt% and 20 wt% were used. For polymer concentration above 20 wt%, the polymer showed a large viscosity, being impossible to reach films with good quality. The polymer was dissolved in DMF for 2 hours at 25 °C under constant magnetic stirring until a homogeneous solution was obtained (step 2 of Fig. 2).

Then, the solution was placed on a clean glass substrate, spread by blade coating with the thickness of 100 μm and placed within an air oven (Binder, ED23) for isothermal solvent evaporation at 25 °C, 50 °C and 100 °C. The samples prepared were identified as (*x*CTFE*y*) where *x* represents the polymer concentration and *y* represents the solvent evaporation temperature.

The initial position of the PVDF-CTFE membranes in the phase diagram studied in this work is represented by the blue stars in the phase diagram of the PVDF-CTFE/DMF system shown in Fig. 2.[29]

The samples studied in this work are representative of the possible phase separation dynamics of the PVDF-CTFE/DMF system as a function of polymer concentration and evaporation temperature, as shown in.[29] This phase diagram presents three main regions: stable, metastable and instable regions separated by the binodal and spinodal lines. The phase separation process (pore size and porosity) occurs in the metastable region, *i.e.*, region between the spinodal and binodal lines. At room temperature, the phase separation process is dominated by nucleation and growth where the samples are located in the metastable region. For PVDF-CTFE concentration below 5 wt%, the mechanical stability of the membranes is very low whereas for polymer concentration above 20 wt% PVDF-CTFE, the viscosity of the system is high, leading to a poor control over the final membrane microstructure.

For a given polymer concentration (*e.g.*, 20 wt% of PVDF-CTFE) but different solvent evaporation temperatures (25 °C, 50 °C and 100 °C), the system goes through the metastable region to the one phase region (homogeneous microstructure), *i.e.*, no liquid–liquid phase separation is observed.

Electrolyte solution uptake and porosity

The electrolyte solution uptake was performed by immersing the membranes for 24 h in a 1 M LiTFSI in PC electrolyte solution, with an ionic conductivity (σ_0) of 6.5×10^{-3} S cm^{-1} at 25 °C.

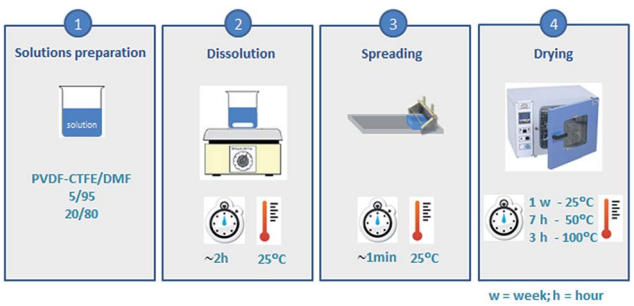

Fig. 1 Experimental procedure for the PVDF-CTFE membrane preparation.

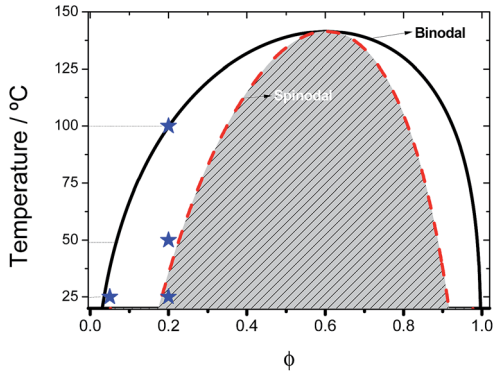

Fig. 2 Phase diagram of the binary PVDF-CTFE/DMF system, after ref. 29.

The uptake value was evaluated according to:

$$\text{uptake} = \frac{m - m_0}{m_0} \times 100 \quad (1)$$

where m_0 is the mass of the dry membrane and m is the mass of the membrane after immersion in the electrolyte solution.

The porosity of the samples (ε) was measured by the pycnometer method:[33]

$$\varepsilon = \frac{W_2 - W_3 - W_s}{W_1 - W_3} \quad (2)$$

where W_1 is the weight of the pycnometer filled with ethanol, W_s is the mass of the sample, W_2 is the weight after the sample was soaked in ethanol and additional ethanol was added to complete the volume of the pycnometer, and W_3 is obtained when the sample was removed from the pycnometer and the residual weight of the pycnometer with ethanol was measured.

The mean porosity of each membrane was obtained as the average of the values determined in three samples.

Characterization techniques

Membranes were coated with a thin gold layer using a sputter coating (Polaron, model SC502 sputter coater) and the cross-section morphology (prepared by fracturing the corresponding film in liquid nitrogen) analyzed using a scanning electron microscope (SEM) (Leica Cambridge apparatus at room temperature).

The polymer crystalline phase was identified by Fourier transform infrared spectroscopy (FT-IR) at room temperature in attenuated total reflectance mode (ATR) with a Jasco FT/IR-4100. FT-IR spectra were collected from 4000 to 600 cm^{-1} after 64 scans with a resolution of 4 cm^{-1}. Thermal properties were determined by differential scanning calorimetry (DSC) with a Mettler Toledo 821e apparatus. The samples were cut from the central region of the membranes, placed in 40 μL crucibles and heated from 25 to 200 °C at a rate of 10 °C min^{-1}, under an argon atmosphere.

Mechanical properties were determined at room temperature in samples with typical dimensions of 10 × 4 mm through stress–strain measurements in the tensile mode of a Shimadzu-AG-IS testing instrument at a strain rate of 1 mm min^{-1}.

Electrochemical properties

Impedance spectroscopy was performed with an Autolab PGSTAT-12 (Eco Chemie) set-up in a frequency range from 65 kHz to 500 mHz, through a constant volume support equipped with gold blocking electrodes located within a Buchi TO 50 oven inside in the glove box. The sample temperature, measured by a type *K* thermocouple, was varied between 20 °C and 100 °C ± 0.5 °C. The ionic conductivity (σ_i) was calculated for each heating cycle thought the following equation:

$$\sigma_i = \frac{d}{R_b A} \quad (3)$$

where R_b is the bulk resistance, d is the thickness and A is the area of the sample.

The tortuosity (τ), the ratio between the effective capillarity and thickness of the sample was determined by:

$$\tau = \sqrt{\frac{\sigma_0 \varepsilon}{\sigma_i}} \quad (4)$$

where σ_0 is the conductivity of the liquid electrolyte, σ_i is the conductivity of the membrane and the electrolyte set at room temperature and ε is the porosity of the membrane.

The MacMullin number, N_m, describes the relative contribution of a separator to cell resistance and is therefore related to the effective conduction process. The MacMullin number, N_m, is defined by:[34]

$$N_m = \frac{\sigma_0}{\sigma_{eff}} \quad (5)$$

where σ_{eff} is the conductivity of the membrane and liquid electrolyte pair and σ_0 is the conductivity of pure liquid electrolyte.

The ionic conductivity temperature dependence follows the Arrhenius equation:

$$\sigma_i = \sigma_0 \exp\left(\frac{-E_a}{RT}\right) \quad (6)$$

where σ_0, is the pre-exponential factor, E_a is the apparent activation energy for ion transport, R is the gas constant (8.314 J mol^{-1} K^{-1}) and T is the temperature.

Lithium cell manufacturing and testing

The electrode was prepared from a slurry of C–$LiFePO_4$ (Phostech Lithium, Lda), carbon black (Super P, Timcal Graphite & Carbon, Switzerland) and PVDF (Binder, Solef 5130, Solvay) in a weight of 8 : 1 : 1 in *N*-methyl-1-pyrrolidone (NMP) solvent. After stirring, the slurry was casted on an aluminum foil through doctor-blade technique and dried at 100 °C for 4 h in a conventional oven, Binder (ED23 oven). The active mass loading of the cathode material was ~2.5 mg cm^{-2}.

All separator membranes studied in this work were immersed in the electrolyte solution (1 M LiTFSI in PC) for 10 minutes within an argon filled glove box (JACOMEX,

Germany) where the moisture and oxygen levels were kept bellow 1.0 ppm.

2032 coin-type Li/C–$LiFePO_4$ half-cells were prepared using the swollen membranes as separators (14 mm diameter), metallic lithium (10 mm diameter) as anode and C–$LiFePO_4$ electrode as cathode (10 mm diameter).

Charge–discharge and cycling tests were carried out at room temperature in the voltage range of 2.0 V and 4.0 V at two different current rates of 0.1C and 2C using a Biologic VMP3 station. The activation cycle was carried out at 0.1C (17 mA g^{-1}) in all cases.

Results and discussion

Morphological and physicochemical properties

Morphology and microstructure of the samples were investigated by SEM images, as the microstructure strongly affects the performance of the battery.[25]

Representative SEM images of the cross-section of the separator membranes are shown in Fig. 3.

For all samples except for the 20CTFE100 a porous morphology is observed with uniform pore features and porosity distribution along the thickness of the samples.

This fact is explained by the position of each sample in the phase diagram of the PVDF-CTFE/DMF system (Fig. 2), as explained in.[29]

The samples show a particulate microstructure in that the spherulitic size depends on the polymer concentration and solvent evaporation temperature.[29]

The porous morphology of the 5CTFE25, 20CTFE25 and 20CTFE50 is due to the lower polymer chains mobility when the solvent is evaporated at a low temperature so that the polymer does not occupy the free space left by the solvent after phase separation.[29]

In relation to the 20CTFE100 sample (Fig. 3d, cross section plus surface morphology of the membrane), the top of the sample shows a slightly different pore structure with pore sizes of around 2 μm resulting from the rapid evaporation of the solvent. On the other hand, the cross-section image of this sample shows a compact structure without the presence of the pores.

The degree of crystallinity, as obtained by differential scanning calorimetry, and β-phase content, as obtained by infrared spectroscopy, of the samples, calculated after the procedures indicated in detail in[29] are summarized in Table 1, together with the degree of porosity.

The degree of crystallinity and β-phase content slightly depend on polymer concentration and solvent evaporation temperature, the variations being therefore not relevant for the influence in battery performance.[12,35]

Table 1 shows that with solvent evaporation at 25 °C, the degree of porosity is between 70% and 60% for polymer concentration between 5 to 20 wt% in the solution.

It is also shown that the degree of porosity decreases with increasing solvent evaporation temperature due to the increase of the solvent evaporation rate, polymer chain mobility and the absence of phase separation process.[29]

For 20CTFE100 sample, the degree of porosity value presented in Table 1 refers only to porosity value in the top layer of the sample.

One of the most relevant parameters in separator membranes is the uptake value once an elevated electrolyte solution content, facilitates ion transport between the two electrodes during the charge and discharge process.[36]

The uptake value of the electrolyte solution for the separator membranes as a function of dipping time is shown in Fig. 4. For all samples, the saturation is achieved after approximately 10 min, with an electrolyte solution content indicating that the void volume of the porous membranes was fully filled.

The correlation between uptake value and degree of porosity is revealed in Fig. 4, *i.e.*, the uptake value increases with increasing the degree of porosity for the PVDF-CTFE membranes with 20 wt% polymer concentration. This fact is also observed in the insert of Fig. 4, showing the correlation between maximum uptake and degree of porosity.

In particular, for solvent evaporation temperature at 25 °C, the highest uptake value (~290%) is observed for the PVDF-CTFE membranes with 20 wt% polymer concentration.

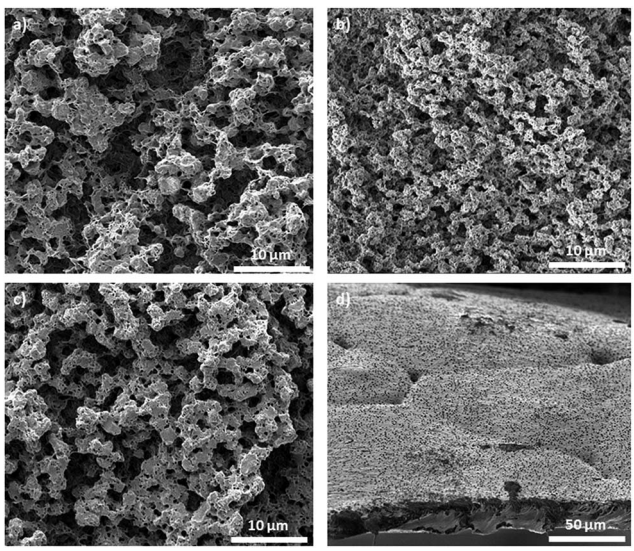

Fig. 3 Cross section SEM images of the membranes prepared from the PVDF-CTFE/DMF solution: solvent evaporation at 25 °C for 5 wt% (a) and 20 wt% (b) of PVDF-CTFE samples. Samples with 20 wt% of PVDF-CTFE with solvent evaporation at 50 °C (c) and 100 °C (d).

Table 1 Degree of porosity, β phase content and degree of crystallinity for the prepared membranes

Samples	Porosity/% ± 5%	β phase/% ± 2%	X/% ± 2%
5CTFE25	71	56	21
20CTFE25	60	33	27
20CTFE50	40	26	25
20CTFE100	35	87	15

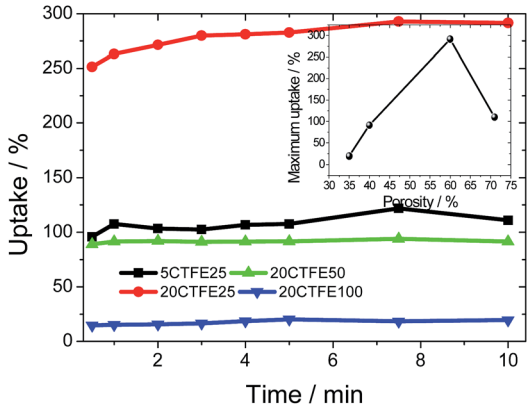

Fig. 4 Electrolyte uptake value as a function of time for the PVDF-CTFE separators samples.

The enhanced interaction between this sample and electrolyte solution is attributed to the initial polymer concentration which is beneficial for cycling performance.[37]

To ensure safe operation of the battery, the mechanical properties of the separator are essential for dimensional stability and to avoid short-circuit and therefore electrical contact between electrodes.[38]

The mechanical properties of the PVDF-CTFE membranes were determined by the stress–strain curves, as represented in Fig. 5.

Fig. 5 shows the stress–strain curves (left) and the Young's modulus (right) of the samples.

All stress–strain curves (Fig. 5a) show the typical characteristics of thermoplastic PVDF polymers, characterized by the elastic and inelastic regions separated by the yielding stress and strain.[39]

As the degree of crystallinity of the samples is similar (Table 1), the differences observed in the mechanical measurements presented in Fig. 5a are fully ascribed to the different microstructures and degree of porosity of the samples (Fig. 1 and Table 1).

Fig. 5b shows the Young's modulus calculated from the strain–stress curves shown in Fig. 5a through the slope in the elastic region at a deformation of 5%.

It is observed that for a given initial polymer concentration in the solutions, 20 wt%, the Young's modulus increases with increasing the solvent evaporation temperature due to a decrease of the degree of porosity.

In relation to a given solvent evaporation temperature, 25 °C, the difference of the Young's modulus within the different two samples is also in agreement with the different porous morphology of the samples (Fig. 1). Finally, the mechanical properties of the samples are suitable for lithium-ion battery applications.

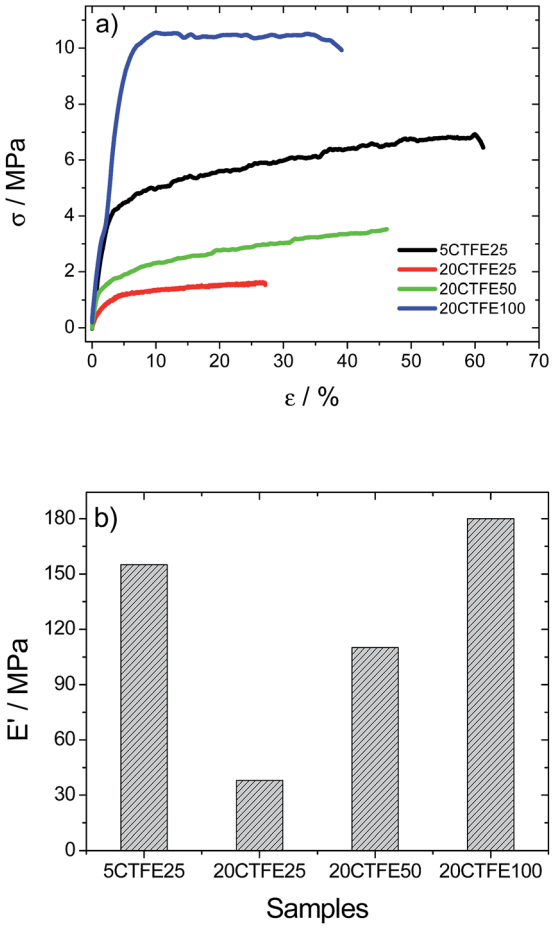

Fig. 5 (a) Stress–strain curves and (b) Young's modulus (E') for the PVDF-CTFE separators samples.

Electrical characteristics of the PVDF-CTFE separator

Impedance spectroscopy measurements were used for the determination of the ionic conductivity of the PVDF-CTFE membranes soaked in the electrolyte solution at different temperatures.

Fig. 6 shows the Nyquist plot at 25 °C for the different PVDF-CTFE separator membranes.

Fig. 6 shows that for the 5CTFE25, 20CTFE25 and 20CTFE50 samples the inclined straight line represents the electrode/electrolyte double layer capacitance behavior.[40]

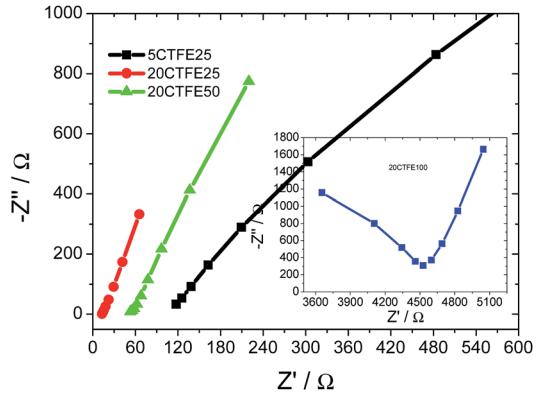

Fig. 6 Nyquist plots for the PVDF-CTFE separators samples.

Table 2 Room temperature ionic conductivity value, tortuosity, MacMullin number (N_m) and activation energy (E_a) for the PVDF-CTFE separator membranes soaked in 1 M LiTFSI-PC

Samples	σ_i/mS cm^{-1}	τ	N_m	E_a/kJ mol^{-1}
5CTFE25	0.06	9.0	108.3	8.0
20CTFE25	1.5	1.6	4.3	4.7
20CTFE50	0.21	5.1	30.9	3.1
20CTFE100	2.8×10^{-3}	28.5	2321.4	9.1

For the 20CTFE100 sample, the Nyquist plot consists of a high frequency semicircle followed by a lower frequency straight line, which correspond to the bulk resistance contribution and the diffusion of lithium ions, respectively.[41]

The disappearance of the high frequency semi-circle for 5CTFE25, 20CTFE25 and 20CTFE50 samples indicates an increase of the total conductivity due to its microstructure and uptake value.[42]

The resistance of the PVDF-CTFE membranes soaked with electrolyte solution has been determined by the intersection of the straight line on the real axis.[25]

The ionic conductivity value for the PVDF-CTFE separator membranes is presented in Table 2, showing ionic conductivity values of above 10^{-4} S cm^{-1} at room temperature, a value that is suitable for lithium battery applications, except for the 20CTFE100 sample.[43]

Table 2 shows that the highest ionic conductivity value is obtained for the PVDF-CTFE separator membrane with the highest electrolyte uptake, *i.e.*, ionic conductivity value is, as expected, mainly determined by the liquid electrolyte uptake, which in turn depends on the degree of porosity of the samples (Table 1).

It also shows the tortuosity value and the MacMullin number (N_m) calculated by eqn (4) and (5), respectively.

The tortuosity value gives information about the conduction process, *i.e.*, the pore connectivity describes a conductivity pathway for the faster ion transport.[12]

The ideal tortuosity value is equal to 1 and describes an ideal porous membrane that corresponds to a perpendicular conduction pathway across the polymer electrolyte.

The value of tortuosity of the PVDF-CTFE separator membranes are between 1.6 and 28.5 depending on the degree of porosity and electrolyte uptake value.

The lower tortuosity value is observed for the 20CTFE25 sample, and is close to the ideal value, which supports better pore connectivity, leading to faster ion transport properties and, consequently, to high battery cycling performance and rate capability.[44]

It is also is observed that the MacMullin number (N_m) is comprehended between 4.3 to 2321.4 which in turn is correlated with the tortuosity value, degree of porosity and electrolyte uptake value of the samples.

The lowest value of the MacMullin number is obtained for the 20CTFE25 sample, with a high degree of porosity, electrolyte uptake and ionic conductivity values and low tortuosity.

Table 3 compares the physicochemical properties of the PVDF-CTFE separator membranes developed in this work with related ones reported in the literature.

The ionic conductivity value determined for the PVDF-CTFE sample is analogous or superior to the values observed for other PVDF separator membranes reported in the literature (Table 3). The differences can be related to the microstructure but also to the degree of porosity and electrolyte uptake value once that the ionic conductivity of the various electrolyte solutions is similar.[49] The difference between the ionic conductivity value for the PVDF-CTFE sample obtained in this work and the other one reported in the literature[26] is related to the processing technique: in the present work, the PVDF-CTFE membrane was produced by solvent casting technique, whereas the one reported in the literature was produced by electrospinning technique. Also the PVDF-CTFE sample produced by electrospinning technique shows high porosity and uptake value but low mechanical properties in comparison of PVDF-CTFE membranes produced in this work.

The electrical conductivity of 1 M LiTFSI in PC *vs.* temperature is illustrated in Fig. 7 and a linear correlation is observed in the temperature range between 25 °C and 100 °C.

This behavior indicates that the ionic conductivity as a function of temperature obeys the Arrhenius model.[50]

The activation energy for ion transportation calculated through the fitting with eqn (6) to the data presented in Fig. 7 is shown in Table 2. The activation energy E_a value is proportional to the ionic conductivity and electrolyte uptake values.

For the 20CTFE25 sample with higher ionic conductivity and electrolyte uptake values, the E_a value is 4.7 kJ mol^{-1}. This low E_a shows the weak dependence of the conductivity on temperature, which is an advantage for battery applications.

Table 3 Ionic conductivity value and degree of porosity for the best PVDF-CTFE sample produced in this work and comparison with other various PVDF separator membranes reported in the literature. The electrolyte solution is also indicated

Samples	σ_i/mS cm^{-1}	Porosity/%	Electrolyte solution	Ref.
PVDF-CTFE	1.5	60	1 M LiTFSI in PC	This work
PVDF-CTFE	2	—	1 M $LiPF_6$ in EC : DMC	26
PVDF-HFP	1.5–2	—	1 M $LiPF_6$ in EC/DEC	45
PVDF-HFP	0.8	—	1 M $LiPF_6$ in EC/PC	46
PVDF	0.13	75	1 M LiTFSI in EC/DEC	47
PVDF	1.4	70	1 M $LiPF_6$ in EC/DMC/EMC	48
PVDF-TrFE	2.6	72	1 M $LiPF_6$ in EC : DMC	25

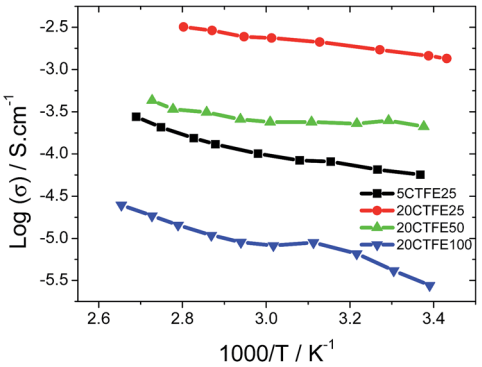

Fig. 7 log σ as a function of 1000/T for the PVDF-CTFE separator membranes.

For the different PVDF-CTFE separator membranes, the ionic conductivity value increases with increasing temperature as observed in Fig. 7. This behavior is partially due to the intrinsic property of liquid electrolytes to increase conductivity upon increasing temperature and to the increase of the free volume and segmental mobility of the polymer with increasing temperature leading to higher ion mobility of the ionic charge carriers.[51]

Further, the heating scan shown in Fig. 7 shows the good stability of the ionic conductivity value for the PVDF-CTFE separator membranes in the temperature range between 25 °C to 100 °C.

Battery tests

The battery performance of the PVDF-CTFE membranes was evaluated in Li/C–$LiFePO_4$ cathodic half-cells at room temperature. The 5CTFE25, 20CTFE25 and 20CTFE50 samples were selected for charge–discharge evaluation taking into account their ionic conductivity value (Fig. 7, Table 2).

Charge–discharge curves of the 5CTFE25 samples in the first cycle at different scan rates from 0.1C to 2C are shown in Fig. 8.

The profiles shown in Fig. 8 are characterized by two pseudoplateaus varying between 3.2 and 3.8 V that depend on the C-rate and reflects the typical electrochemical behavior of the

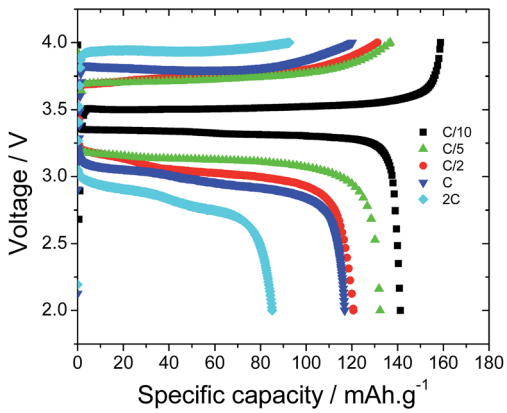

Fig. 8 Charge–discharge profiles for 5CTFE25 at different scan rates.

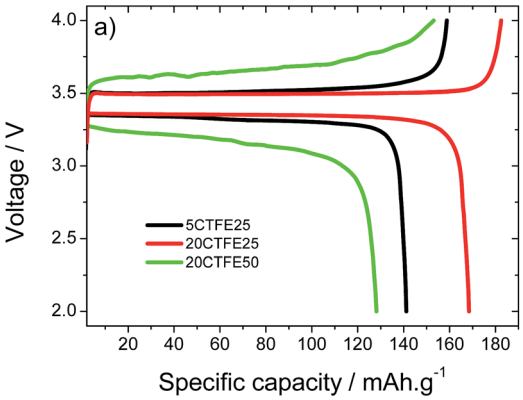

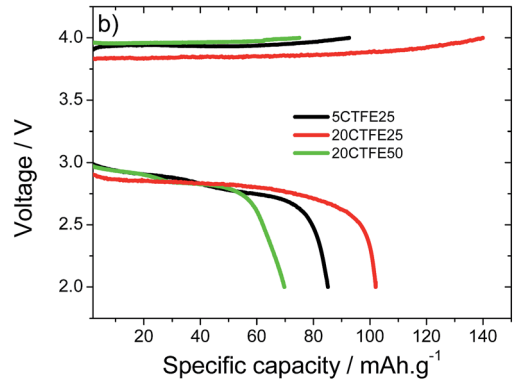

Fig. 9 Charge–discharge profiles for the PVDF-CTFE separator membranes at (a) C/10 and (b) 2C.

C–LiFePO4 spinel for the reversible charge (lithium removal)–discharge (lithium insertion) cycling process.

Through Fig. 8, the discharge capacity is 142 mA h g^{-1}, 132 mA h g^{-1}, 121 mA h g^{-1}, 117 mA h g^{-1}, and 85 mA h g^{-1} at rates of C/10, C/5, C/2, C and 2C, respectively.

Fig. 8 also shows that the voltage and discharge capacity value decreases progressively as the C-rates increase, which is a result of the significant influence of ionic transport on ohmic polarization.[40]

The charge–discharge behavior as a function of different C-rates for the 5CTFE25 sample is representative to the one observed for the other two samples.

Fig. 9 depicts a comparison of the room temperature charge–discharge curves at C/10 (Fig. 9a) and 2C (Fig. 9b) for the half-cell containing the different PVDF-CTFE separator membranes.

At C/10 (Fig. 9a), half-cells using 20CTFE25, 5CTFE25 and 20CTFE50 showed stable charge–discharge profiles with discharge capacity about 168 mA h g^{-1}, 142 mA h g^{-1} and 127 mA h g^{-1}, respectively. Also for 2C (Fig. 9b), it is observed a cycling behavior similar to C/10 but with lower discharge capacity value. For 2C, the discharge capacity value is 102 mA h g^{-1}, 85 mA h g^{-1} and 69 mA h g^{-1} for 20CTFE25, 5CTFE25 and 20CTFE50 samples, respectively.

The discharge capacity value of the 20CTFE25 sample is higher in comparison to the other PVDF-CTFE separator membranes (5CTFE25 and 20CTFE50 samples) for low (C/10)

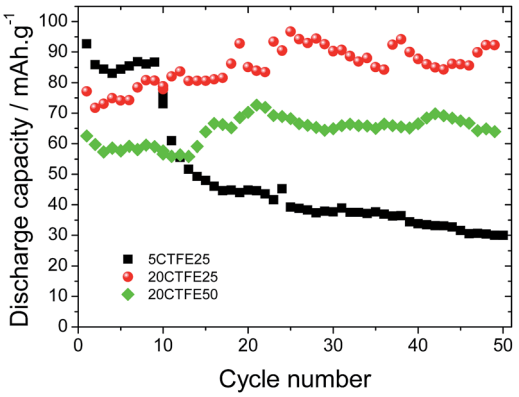

Fig. 10 Cycling performance of C–LiFePO4 cathodic half cells containing the different PVDF-CTFE separator membranes at 2C.

and high (2C) C- rates. This fact is due to the higher conduction of Li^+ ions (ionic conductivity value) resulting from the higher electrolyte uptake value of the 20CTFE25 samples.

The cycling performance of the C–$LiFePO_4$ half-cells is shown in Fig. 10. For half cells containing 20CTFE25, 20CTFE50 and 5CTFE25 samples, the discharge capacity values after 50 cycles are 92 mA h g^{-1}, 64 mA h g^{-1} and 30 mA h g^{-1}, respectively.

The corresponding capacity retentions after 50 cycles is 54%, 38% and 18%, respectively. The capacity retentions were calculated based on the theoretical capacity, 170 mA h g^{-1}, of C–$LiFePO_4$.

The higher discharge value and capacity retention after 50 cycles of the half-cell with 20CTFE25 sample is attributed to the higher ionic conductivity and electrolyte uptake value that facilitates the repeated lithium ion insertion/de-insertion in/from the C–$LiFePO_4$ electrodes even at high C rate, as demonstrated in Fig. 10.

In conclusion, the 20CTFE25 sample shows high discharge capacity value with high rate capability. However, it is observed in Fig. 10 at 2C (charge and/or discharge process in half an hour), that the battery with the 20CTFE25 membrane shows a discharge value of 92 mA h g^{-1}, which is still 54% of the theoretical value, which indicates the good performance of the battery.

Conclusions

Separator membranes of poly(vinylidene fluoride-*co*-chlorotrifluoroethylene) (PVDF-CTFE) have been prepared by solvent casting through its phase diagram with *N*,*N*-dimethylformamide (DMF) solvent. Different morphologies have been obtained varying initial polymer concentration in the solution and solvent evaporation temperature. A porous microstructure is achieved for PVDF-CTFE membranes with solvent evaporation temperature up to 50 °C.

The mechanical properties of the PVDF-CTFE separator membranes are suitable for lithium-ion batteries and are correlated with degree of porosity and microstructure if the membranes. Also the ionic conductivity value depends on the degree of porosity and electrolyte uptake value. The best ionic conductivity value at room temperature is 1.5 mS cm^{-1} for the membrane prepared with 20 wt% initial polymer concentration and solvent evaporation temperature at 25 °C, leading to a degree of porosity of 60% and an electrolyte uptake value of 292%.

The prepared PVDF-CTFE separator membranes show good cyclability and rate capability. At C/10 and 2C presents the discharge values are 168 and 102 mA h g^{-1}, respectively. PVDF-CTFE separators are thus excellent candidate for their use in high-power and safety lithium-ion batteries applications.

Acknowledgements

This work is funded by FEDER funds through the "Programa Operacional Factores de Competitividade – COMPETE" and by national funds from FCT – Fundação para a Ciência e a Tecnologia, in the framework of the strategic project Strategic Project PEST-C/FIS/UI607/2014 and PEST-C/QUI/UI0686/2013. A. G. and C. M. C. also thanks the FCT for the grant SFRH/BD/90313/2012 and SFRH/BPD/112547/2015, respectively.

Notes and references

1 R. Huggins, *Advanced Batteries: Materials Science Aspects*, Springer, 2008.
2 P. G. Bruce, B. Scrosati and J.-M. Tarascon, *Angew. Chem., Int. Ed.*, 2008, **47**, 2930–2946.
3 J.-M. Tarascon, *Philos. Trans. R. Soc., A*, 2010, **368**, 3227–3241.
4 J. M. Tarascon and M. Armand, *Nature*, 2001, **414**, 359–367.
5 W. A. van Schalkwijk and B. Scrosati, *Advances in Lithium-Ion Batteries*, Kluwer Academic/Plenum Publishers, 2002.
6 M. Wakihara and O. Yamamoto, *Lithium Ion Batteries: Fundamentals and Performance*, John Wiley & Sons, 2008.
7 K. E. Aifantis, S. A. Hackney and R. V. Kumar, *High Energy Density Lithium Batteries: Materials, Engineering, Applications*, John Wiley & Sons, 2010.
8 X. Huang, *J. Solid State Electrochem.*, 2011, **15**, 649–662.
9 P. B. Balbuena and Y. Wang, *Lithium-Ion Batteries: Solid-Electrolyte Interphase*, Imperial College Press, 2004.
10 K. H. J. Buschow, *Encyclopedia of materials: science and technology*, Elsevier, 2001.
11 L.-L. Zhang, Z.-L. Wang, D. Xu, X.-B. Zhang and L.-M. Wang, *Int. J. Smart Nano Mater.*, 2012, 1–20, DOI: 10.1080/19475411.2012.659227.
12 C. M. Costa, M. M. Silva and S. Lanceros-Mendez, *RSC Adv.*, 2013, **3**, 11404–11417.
13 J. Luo, O. Conrad and I. F. J. Vankelecom, *J. Mater. Chem. A*, 2013, **1**, 2238–2247.
14 J. Luo, A. H. Jensen, N. R. Brooks, J. Sniekers, M. Knipper, D. Aili, Q. Li, B. Vanroy, M. Wübbenhorst, F. Yan, L. V. Meervelt, Z. Shao, J. Fang, Z.-H. Luo, D. E. De Vos, K. Binnemans and J. Fransaer, *Energy Environ. Sci.*, 2015, **8**, 1276–1291.
15 P. Arora and Z. Zhang, *Chem. Rev.*, 2004, **104**, 4419–4462.
16 H. Lee, M. Yanilmaz, O. Toprakci, K. Fu and X. Zhang, *Energy Environ. Sci.*, 2014, **7**, 3857–3886.

17 V. Deimede and C. Elmasides, *Energy Technol.*, 2015, **3**, 453–468.
18 A. Manuel Stephan and K. S. Nahm, *Polymer*, 2006, **47**, 5952–5964.
19 F. S. Fiory, F. Croce, A. D'Epifanio, S. Licoccia, B. Scrosati and E. Traversa, *J. Eur. Ceram. Soc.*, 2004, **24**, 1385–1387.
20 A. I. Gopalan, P. Santhosh, K. M. Manesh, J. H. Nho, S. H. Kim, C.-G. Hwang and K.-P. Lee, *J. Membr. Sci.*, 2008, **325**, 683–690.
21 O. Bohnke, G. Frand, M. Rezrazi, C. Rousselot and C. Truche, *Solid State Ionics*, 1993, **66**, 97–104.
22 Z. Zhong, Q. Cao, B. Jing, X. Wang, X. Li and H. Deng, *Mater. Sci. Eng., B*, 2012, **177**, 86–91.
23 A. Magistris, E. Quartarone, P. Mustarelli, Y. Saito and H. Kataoka, *Solid State Ionics*, 2002, **152–153**, 347–354.
24 R. E. Sousa, J. Nunes-Pereira, C. M. Costa, M. M. Silva, S. Lanceros-Méndez, J. Hassoun, B. Scrosati and G. B. Appetecchi, *J. Power Sources*, 2014, **263**, 29–36.
25 C. M. Costa, J. L. Gomez Ribelles, S. Lanceros-Méndez, G. B. Appetecchi and B. Scrosati, *J. Power Sources*, 2014, **245**, 779–786.
26 F. Croce, M. L. Focarete, J. Hassoun, I. Meschini and B. Scrosati, *Energy Environ. Sci.*, 2011, **4**, 921–927.
27 M. Xiong, H. Tang, Y. Wang and M. Pan, *Carbohydr. Polym.*, 2014, **101**, 1140–1146.
28 M. Xiong, H. Tang, Y. Wang, Y. Lin, M. Sun, Z. Yin and M. Pan, *J. Power Sources*, 2013, **241**, 203–211.
29 R. E. Sousa, J. C. C. Ferreira, C. M. Costa, A. V. Machado, M. M. Silva and S. Lanceros-Mendez, *J. Polym. Sci., Part B: Polym. Phys.*, 2015, **53**, 761–773.
30 M. Zaccaria, C. Gualandi, D. Fabiani, M. L. Focarete and F. Croce, *J. Nanomater.*, 2012, **2012**, 8.
31 H. Lee, M. Alcoutlabi, J. V. Watson and X. Zhang, *J. Polym. Sci., Part B: Polym. Phys.*, 2013, **51**, 349–357.
32 M. Alcoutlabi, H. Lee, J. Watson and X. Zhang, *J. Mater. Sci.*, 2013, **48**, 2690–2700.
33 A. California, V. F. Cardoso, C. M. Costa, V. Sencadas, G. Botelho, J. L. Gómez-Ribelles and S. Lanceros-Mendez, *Eur. Polym. J.*, 2011, **47**, 2442–2450.
34 K. K. Patel, J. M. Paulsen and J. Desilvestro, *J. Power Sources*, 2003, **122**, 144–152.
35 J. Nunes-Pereira, C. M. Costa and S. Lanceros-Méndez, *J. Power Sources*, 2015, **281**, 378–398.
36 W.-K. Shin, J.-H. Yoo and D.-W. Kim, *J. Power Sources*, 2015, **279**, 737–744.
37 J. Shi, H. Hu, Y. Xia, Y. Liu and Z. Liu, *J. Mater. Chem. A*, 2014, **2**, 9134–9141.
38 J. Cannarella, X. Liu, C. Z. Leng, P. D. Sinko, G. Y. Gor and C. B. Arnold, *J. Electrochem. Soc.*, 2014, **161**, F3117–F3122.
39 C. M. Costa, V. Sencadas, I. Pelicano, F. Martins, J. G. Rocha and S. Lanceros-Mendez, *J. Non-Cryst. Solids*, 2008, **354**, 3871–3876.
40 W. Xiao, L. Zhao, Y. Gong, S. Wang, J. Liu and C. Yan, *RSC Adv.*, 2015, **5**, 34184–34190.
41 B.-Y. Chang and S.-M. Park, *Annu. Rev. Anal. Chem.*, 2010, **3**, 207–229.
42 J. Malathi, M. Kumaravadivel, G. M. Brahmanandhan, M. Hema, R. Baskaran and S. Selvasekarapandian, *J. Non-Cryst. Solids*, 2010, **356**, 2277–2281.
43 J. Hassoun, D.-J. Lee, Y.-K. Sun and B. Scrosati, *Solid State Ionics*, 2011, **202**, 36–39.
44 G. Venugopal, J. Moore, J. Howard and S. Pendalwar, *J. Power Sources*, 1999, **77**, 34–41.
45 Y. Wang, J. Travas-Sejdic and R. Steiner, *Solid State Ionics*, 2002, **148**, 443–449.
46 J. M. Tarascon, A. S. Gozdz, C. Schmutz, F. Shokoohi and P. C. Warren, *Solid State Ionics*, 1996, **86–88**(1), 49–54.
47 Y. Saito, H. Kataoka, E. Quartarone and P. Mustarelli, *J. Phys. Chem. B*, 2002, **106**, 7200–7204.
48 G.-L. Ji, B.-K. Zhu, Z.-Y. Cui, C.-F. Zhang and Y.-Y. Xu, *Polymer*, 2007, **48**, 6415–6425.
49 A. Gören, C. M. Costa, M. M. Silva and S. Lanceros-Méndez, *Composites, Part B*, 2015, **83**, 333–345.
50 C. M. Costa, L. C. Rodrigues, V. Sencadas, M. M. Silva and S. Lanceros-Méndez, *Solid State Ionics*, 2012, **217**, 19–26.
51 F. M. Gray, *Polymer Electrolytes*, Royal Society of Chemistry, 1997.

